Minimizing Charging Delay for Directional Charging in Wireless Rechargeable Sensor Networks

Chi Lin*†, Yanhong Zhou*†, Fenglong Ma‡, Jing Deng§, Lei Wang*†, and Guowei Wu*†
*School of Software Technology, Dalian University of Technology, Liaoning, Dalian 116023, China
†Key Laboratory for Ubiquitous Network and Service Software of Liaoning Province, Dalian, 116621, China
‡Department of Computer Science and Engineering, University at Buffalo, NY, 14221, U.S.A.
§Department of Computer Science, University of North Carolina at Greensboro NC 27412, U.S.A.
Emails: {c.lin,wgwdut}@dlut.edu.cn, zyhali37@gmail.com, fenglong@buffalo.edu, jing.deng@uncg.edu, lei.wang@ieee.org

***Abstract*—The discovery of Wireless Power Transfer (WPT) technologies makes charging more convenient and reliable. Among all the existing WPT technologies, directional WPT is more efficient and has been successfully applied to supply energy for wireless rechargeable sensor networks (WRSNs). However, the state-of-the-art methods ignore the anisotropic energy receiving property of rechargeable sensors, resulting in energy wastage. In order to address this issue, in this paper, we point out that the received energy of a sensor is not only relative to the distance, but also relative to the angle between the sensor and the charger's orientation in directional WPT. Towards this end, we derive a pragmatic energy transfer model verified by experiments. In particular, we focus on a Minimal chArging Delay (MAD) problem to reduce charging delays. To obtain the optimal solution, we formulate the problem as a linear programming problem. Moreover, we introduce a method of charging power discretization, which significantly reduces the search space and bounds the performance gap to the optimal one with a $\frac{1}{1-\epsilon^2}$ approximation ratio. Besides, a merging method is introduced for a more practical application scenario. Finally, we demonstrate that our methods outperform the Set Cover baseline method by an average of 34.2% through simulations and experiments.**

I. Introduction

Wireless power transfer (WPT) technologies have slowly changed the ways we use battery-powered devices since Kurs et al. [1] demonstrated that efficient power can be transmitted between magnetically resonant coils in a strongly coupled regime. Currently, many WPT technologies have been developed, such as magnetic resonant coupling [1], inductive coupling [2], and electro-magnetic radiation [3]. With these enabling technologies, wireless rechargeable sensor networks (WRSNs) become a promising platform for various applications, such as wearable devices [4], access authentication [5], and urban sensing [6]–[9]. In a WRSN implementing with WPT technology, the charger acts as the energy transmitter, and the rechargeable sensors or devices act as energy receivers. However, relatively low energy transfer efficiency of WPT technologies still limits WRSNs' widespread adoptation.

One approach to improve efficiency is to use directional WPT [10]. Differing from omnidirectional WPT [11], the energy transmitter in directional WPT aggregates the radiated energy in limited directions via energy beamforming [12]. Accordingly, the energy receivers can only receive non-negligible energy when they are located in the covered regions of the energy transmitter.

Existing literatures mainly focus on optimizing the performance of network that adopts omnidirectional WPT [13]–[15]. In practice, chargers with omnidirectional WPT will broadcast the electromagnetic waves equally in all directions. Since the radiated energy fades rapidly over distance, chargers might require excessively high transmit power to charge a sensor, which will invest extensive energy cost for network operating. Therefore, directional WPT is more accurate in charging although more careful designs will be needed.

One of such design details is the antenna theory that needs to be thoroughly investigated. The energy collected by the receiver antenna is proportional to the effective area in which it is exposed to the radiated electromagnetic waves [16]. Since the orientation of the charger is arbitrary, it will dramatically change the effective area. In other words, the amount of received energy at each sensor's antenna changes with the angle between the line from the sensor to the charger and the charger antenna's orientation, i.e., the anisotropic energy receiving property of rechargeable sensors. For example, within the covered region of TX91501 Powercast wireless charger, the maximal received energy of a rechargeable sensor is $49mW$ and the minimal value is $9mW$.

Although there are a few studies focusing on the charging problem of WRSN adopting directional WPT [17], none of them considers the anisotropic energy receiving property of directional charging for practical applications. In general, to save the energy expenditure that maintains a network operation in the real application scenarios, it is essential to formulate an energy transfer model taking angle information into account and obtain the charging orientation solution for chargers.

In this paper, we mainly focus on exploring the attenuation with distance and variation with angles of the received energy for sensors. Then, we define the following Minimal chArging Delay (MAD) problem to reduce charging delays. In the network settings that we consider, a mobile charger (MC) travels and stops at several planned locations to wirelessly charge its surrounding sensors. Since directional charging is used, we are facing two main technical challenges. The first challenge is to formulate the energy transfer model with both distance and angle; and the second is to design a solution to

bound the performance gap to the optimal one and reduce the computational complexity in the meanwhile.

The main contributions of this work are summarized as below.

- To the best of our knowledge, we are the first to formulate the energy transfer model with two influential factors (i.e., distance and angle) in directional charging WRSNs. We propose a practical energy transfer model based on the well-known Friis's free space model. Experimental results demonstrate and validate the feasibility and practicability of the proposed model.
- We formulate the sojourn planning problem as a MAD problem, which can be solved with linear programming.
- In order to reduce the computational complexity, we design the charging power discretization method, which significantly reduces the search space and bounds the charging delay to the linear programming solution by $\frac{1}{1-\epsilon^2}$, where ϵ is a power difference threshold. We further propose a merging technique to combine neighboring charging sections to reduce charging delay.
- We have performed simulations and testbed experiments to evaluate our designs with a baseline Set Cover solution. Our designs have been demonstrated with superior performances.

The rest of this paper is organized as follows. Section II surveys the state-of-the-art literature on WRSNs. Section III illustrates the network model, charging models, and problem definitions. Section IV presents a charging power discretization and orientation angle merging method for MAD in detail. Section V and VI evaluate our design via simulations and experiments. Finally, Section VII concludes our work.

II. Literature Review

WPT technology significantly promotes the development of WRSNs in recent years. In general, previous arts can be classified into two types based on behaviors and functionalities of chargers: stationary charging [17]–[19] and mobile charging [13], [14], [20]–[24].

In *stationary charging*, wireless chargers are fixed at several positions to replenish energy for sensor nodes. Most studies on stationary charging concentrate on the placement of chargers. Zhang et al. [18] solved a charger placement and power allocation problem to optimize charging quality, subjected to a limited power budget. Li et al. [19] proposed a cooperatively deployment technique with minimum number of chargers and sink stations. Different from the above aspects, Dai et al. [17] concentrated on the charger placement with optimized charging utility by determining charging locations as well as orientations for chargers. The potential security problem caused by RF exposure was investigated in [25]. Overall, stationary charging techniques suffer from the issue of higher cost and limited coverage.

Different from stationary charging, *mobile charging* focuses on scheduling a small number of chargers to replenish energy for sensor nodes by traveling through the network and the charging problem is transformed into the issue of trip planning. In order to minimize the total charging delay, Fu et al. [13] tried to find the optimum sojourn location and time for mobile chargers. Lin et al. [20], [24] concentrated on promoting network lifetime and energy efficiency. Shu et al. [21] focused on charging energy maximization and optimized charger travel speed. Han et al. [26] tried to balance charger energy expenditure and eventual energy reception at sensor nodes with a grid-based joint routing and charging technique. Xie et al. [23] proposed algorithms to jointly consider traveling path, flow routing, and charging time to maximize the time that charger spent at the service station. To minimize the sum of movement energy and loss energy, Zhang et al. [14] presented the itinerary selection and charging association problem and designed heuristic algorithms to solve it. Similarly, Sangare et al. [27] chose the itinerary for traveling and scheduled a subset of sensor nodes to charge by applying Markov decision process.

Nevertheless, little attention has been paid on directional charging [17] that allows more efficient charging. It is an important issue in the practical applications even though a more careful investigation would be needed.

III. Preliminaries

A. Network Model and Charging Model

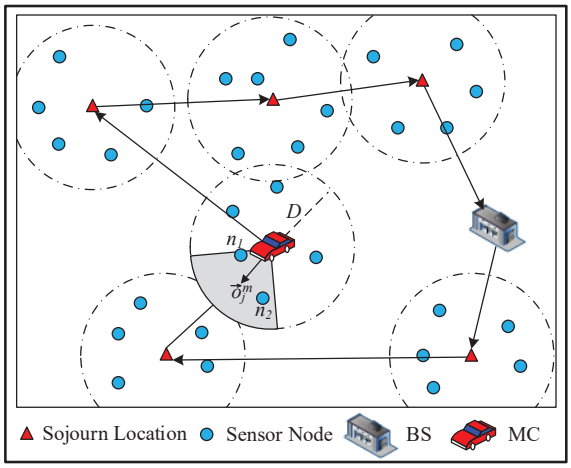

Fig. 1. Overview of the network model.

As shown in Figure 1, we suppose a network is deployed with N wireless rechargeable sensor nodes, and we can localize each node n_i in the network using technologies such as [28] and represent the location as $\vec{n_i}$=(x_i,y_i). Since the radiated energy of MC fades rapidly over distance, only the sensors locating in a circle with a radius of D can receive non-negligible energy. Hence, MC travels and stops at several predefined locations to wirelessly charge its surrounding sensors. When MC stops at the m-th location and charges with the j-th orientation angle, its orientation $\vec{o_j^m}$ can vary from 0 to 2π. Only the nodes located in the covered area can be charged, i.e., n_1 and n_2 in Figure 1. After charging all nodes, MC will return back to base station (BS) for a quick battery replacing

service. For a quick reference, we list the main notations used in this paper in Table I.

TABLE I
MAIN NOTATIONS FOR QUICK REFERENCE

Symbols	Definitions
N	Number of sensor nodes.
M	Number of sojourn locations for a MC.
A	Number of alternative orientation angles for a MC.
m	Mobile charger.
n_i	Sensor node i.
$\vec{o_j}$	Orientation angle vector of a MC at the j-th orientation.
$\vec{n_i}$	Directional vector of sensor node i.
α	Angle between a MC and a sensor node.
D	Longest effective transfer distance of a MC.
C_e	A circle with a radius of D.
d_{im}	Distance between a MC and node i.
δ_i	Energy threshold of sensor node i.
E_S	Total energy of a sensor node.
P_{ij}^m	Charging power for node i with j-th orientation angle at m-th sojourn location.
t_j^m	Charging delay with j-th orientation angle at m-th sojourn location.

First, we give an illustration of directional charging. In Figure 2, nodes n_i and n_k are covered by an effective directional area when the orientation of MC is $\vec{o_j}$. They will receive different energy amount under different angle α_i, α_k and distance d_i and d_j, respectively. Nevertheless, when MC rotates to $\vec{o_l}$, these two nodes cannot receive energy anymore. Hence, in directional charging, the received energy has two influence factors: distance and angle. The energy transfer model can be expressed as $P_r = f(d, \alpha)$.

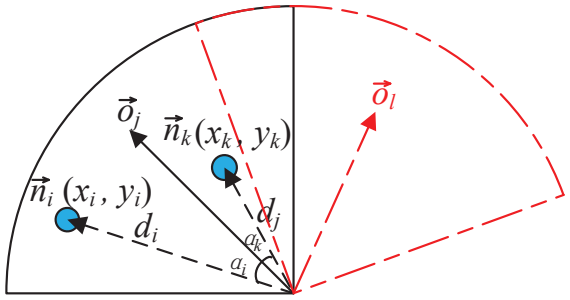

Fig. 2. Directional charging model.

To formulate the energy transfer model, we first introduce Friis's free space equation:

$$P_r = G_s G_r (\frac{\lambda}{4\pi d})^2 P_0 \ , \tag{1}$$

which expresses the received energy P_r, d-distance away from the energy transmitter with source energy P_0. In (1), G_s and G_r represent the source antenna gain and receive antenna gain, respectively. Then, He et al. [11] gave an empirical model of wireless recharging in WRSN as follows:

$$P_r = \frac{G_s G_r \eta}{L_p} (\frac{\lambda}{4\pi(d+\beta)})^2 P_0, \tag{2}$$

where η is rectifier efficiency, L_p represents poloarization loss, and β is a parameter to adjust the Friis's free space equation for short distance transmission. According to the antenna theory, (1) can be expressed according to the concept of effective area:

$$P_r = A_{er} \cdot S_r = \frac{P_0 G_t A_{er}}{4\pi d^2} \ , \tag{3}$$

where A_{er} is the effective receiving area, and S_r refers to power density at receiving antenna. Moreover, the source antenna gain G_t can be expressed as:

$$G_t = \frac{4\pi A_{et}}{\lambda^2} \ . \tag{4}$$

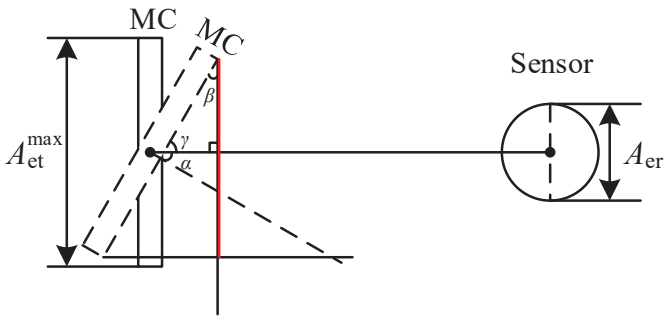

Fig. 3. Directional charging schematic.

As depicted in Figure 3, in our scenario, A_{er} is the effective receiving area of a sensor node, and A_{et} is the effective transferring area of MC. When MC is facing the sensor node (i.e., the angle between sensor and MC is 0), the effective transferring area A_{et} is the largest which is denoted as A_{et}^{max}. When the angle between MC and sensor is α, the effective transferring area is $A_{et} = A_{et}^{max} cos\beta$. We can easily prove that $\alpha = \beta$, hence, $A_{et} = A_{et}^{max} cos\alpha$.

Now, we can derive an energy transfer model by combining the above equations:

$$P_r = \frac{G_t G_r \eta}{L_p} (\frac{\lambda}{4\pi(d+\beta)})^2 P_0 = \frac{\eta A_{er} A_{et}^{max} cos\alpha}{L_p \lambda^2 (d+\beta)^2} P_0 \ . \tag{5}$$

Then, we give an experimental energy transfer model:

$$P_r = \frac{\eta A_{er} A_{et}^{max} (cos\alpha + c)}{L_p \lambda^2 (d+\beta)^2} P_0 \ , \tag{6}$$

where c is a parameter to adjust the equation for vertical situation, i.e., $\alpha = \pm\frac{\pi}{2}$. To simplify the description of the following design, we express the experimental energy transfer model as:

$$P_r = \mu \frac{cos\alpha + c}{(d+\beta)^2} \ , \tag{7}$$

where c, μ and β are constants which are determined by the experimental environment and the hardware parameters of chargers [11].

We perform experiments to verify the energy transfer model. We use an off-the-shelf TX91501 Powercaster wireless charger and Powercast wireless rechargeable sensor nodes in our lab. First, we adopt (7) to fit the experimental data. The fitting

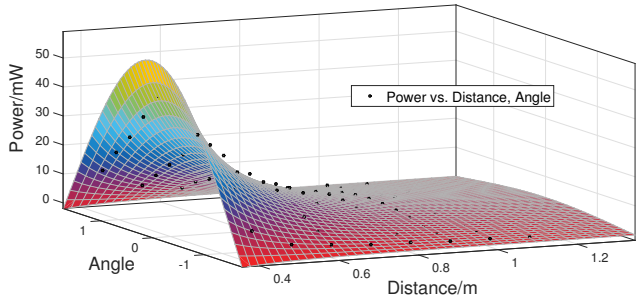

Fig. 4. Comparing experimental results (black dots) and fitted results (mesh). Fitted results are based on $c = 0.1161$, $\mu = 3.893$, and $\beta = 0.1$

results are shown in Figure 4 proving that (5) is practical in our experimental environments. Then, we fix the charger's orientation angle with respect to the line connecting the charger and the node, and vary the distance between the charger and the node from $0.4m$ to $1.1m$. Finally, we change the charger's orientation angle from $-\pi$ to π under different distance. The experimental results are shown in Figure 5 and Figure 6, respectively. Figure 6 verifies the anisotropic energy receiving property of rechargeable sensors.

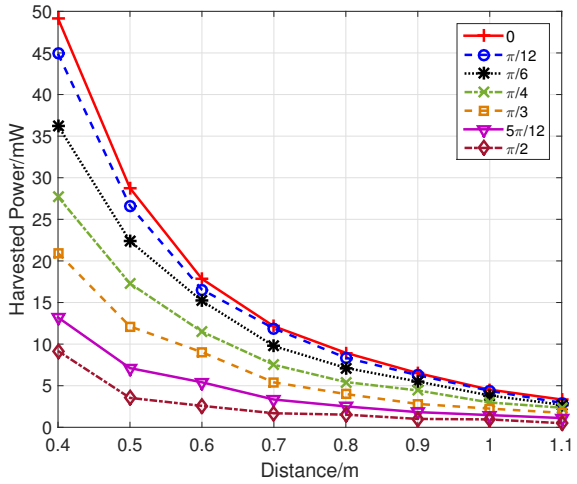

Fig. 5. Receiving power vs. distance.

The experimental results reveal two insights: First, the sensor node can only receive non-negligible energy when the orientation angle is within $-\frac{\pi}{2}$ to $\frac{\pi}{2}$, i.e., $\alpha \in [-\frac{\pi}{2}, \frac{\pi}{2}]$. Second, the sensor node harvests little energy when the distance is longer than $1m$. Hence, we set the effective charging distance D of MC as $1m$ and define the circle with a radius of D as an effective charging area C_e.

Based on these experimental results and (7), the charging power transmitted from the charger m to a sensor node n_i can be given by :

$$P_r(d,\alpha) = \begin{cases} \mu\frac{cos\alpha+c}{(d+\beta)^2}, & 0 \le d \le D, \frac{-\pi}{2} \le \alpha \le \frac{\pi}{2} \\ 0, & \text{otherwise.} \end{cases}$$

$$d = ||mn_i||, \alpha = arccos(\frac{\vec{o_j}\vec{n_i}}{|\vec{o_j}\vec{n_i}|}) \ , \tag{8}$$

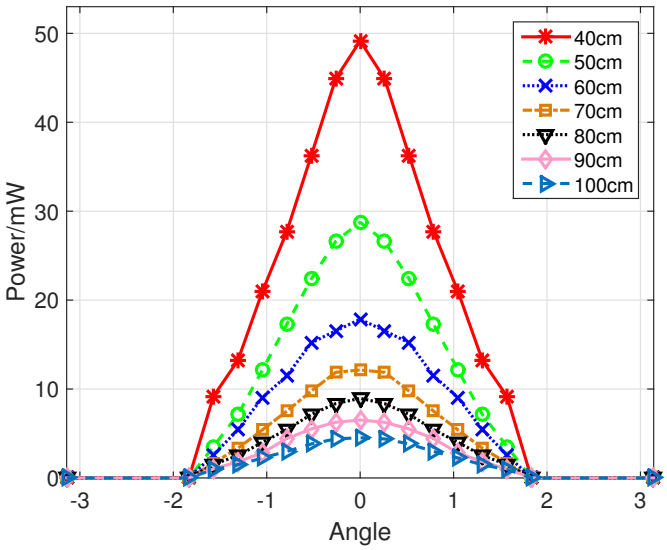

Fig. 6. Receiving power vs. angle.

where d refers to the distance between m and n_i, and α denotes the angle between $\vec{o_j}$ and $\vec{n_i}$,

B. Problem Formulation

Our goal here is to minimize the total charging delay for all sensor nodes in the network to promote energy efficiency and support nodes to complete their sensing, communication, and computation in the meanwhile. To achieve this goal, we define a Minimal chArging Delay (MAD) problem and seek the solution that contains optimal orientation and corresponding charging delay for MC. We formulate the MAD problem as below.

$$\min T = \sum_{m=1}^{M}\sum_{j=1}^{A} t_j^m \ , \tag{9}$$

Subject to :

$$\sum_{m=1}^{M}\sum_{j=1}^{A} P_{ij}^m t_j^m \ge \delta_i E_s, \ \forall i \in N \ , \tag{10}$$

$$P_{ij}^m = P_r(d_{im}, \alpha_{ij}) \ . \tag{11}$$

In (9), t_j^m denotes the charging delay when MC stops at the m-th location with the j-th orientation angle. Eq. (10) means that MC needs to replenish the energy above the threshold $\delta_i E_s$ for each node to make it work normally. Here, P_{ij}^m refers to the harvested power of node i during t_j^m charging delay.

IV. Proposed Technique

Since the MAD problem has been formulated as a Linear Programming (LP) problem, we can brute force all possible orientation angles to find the optimal strategies and solve it by applying LP solver [29]. Nevertheless, the orientation angles can be ranged from 0 to 2π (see Figure 7), and it will cost heavy computational overhead which is not suitable for practical applications. Hence, we introduce the charging power

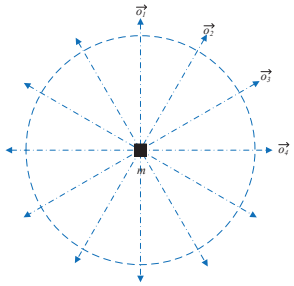

Fig. 7. Illustration of orientation angles.

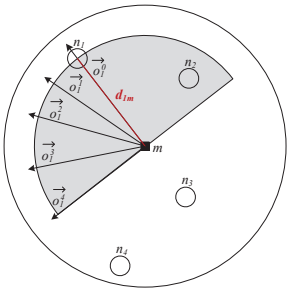

Fig. 8. Discretizing charging power for node n_1.

discretization and merging method. Moreover, we bound the performance gap based on the optimal solution.

A. Charging Power Discretization

Inspired by the discretizing charging power method based on the charging distance [13], [21], we adopt the same theory to discretize charging power based on angles. When MC stops at a location m, only the nodes that are located in the effective charging area C_e can receive notable energy. Furthermore, a node n_i will receive different power when the angle and distance between MC and itself vary (see Figure 5 and 6). Since a node can only receive non-negligible energy when the angle is within the range from $-\frac{\pi}{2}$ to $\frac{\pi}{2}$, the minimal and maximal angles between a node n_i and MC are $\alpha_i^{min} = 0$ and $\alpha_i^{max} = \frac{\pi}{2}$, respectively. Combining this range of angles and (7), we can calculate the corresponding charging power range:

$$P_i^{max} = \mu \frac{cos0 + c}{(d_{im} + \beta)^2} = \frac{\mu(1+c)}{(d_{im} + \beta)^2} \ , \tag{12}$$

$$P_i^{min} = \mu \frac{cos\frac{\pi}{2} + c}{(d_{im} + \beta)^2} = \frac{\mu c}{(d_{im} + \beta)^2} \ . \tag{13}$$

To discretize the charging power at node n_i, we use V_i to denote the number of vectors that start from the sojourn location of MC. The charging power at the v-th vector is denoted as P_i^v. Specifically, the difference of charging power between neighboring vectors is less than a threshold factor ϵ $(0 < \epsilon < 1)$, i.e.,

$$P_i^v = (1+\epsilon) P_i^{v+1} \ , \tag{14}$$

where P_i^v can be calculated as below:

$$P_i^v = P_i^{max}(1+\epsilon)^{-v}, \ 1 \le v \le V_i \ . \tag{15}$$

The total number of vectors V_i is simultaneously decided by the last power vector which is greater than P_i^{min}, the two border line orientations (i.e., $-\frac{\pi}{2}, \frac{\pi}{2}$), and an orientation that MC faces to n_i. Moreover, the charging power is a symmetric function about angles. Consequently, V_i can be calculated by the following equation:

$$V_i = 2\lfloor \frac{ln(\frac{P_i^{max}}{P_i^{min}})}{ln(1+\epsilon)} + 1 \rfloor + 1 = 2\lfloor \frac{ln(\frac{1}{c}+1)}{ln(1+\epsilon)} + 1 \rfloor + 1 \ . \tag{16}$$

We give an example of discretizing power for n_1 in Figure 8. The charging power at the direction of $\vec{o_1^0}$ is the maximum, i.e., $P_1^0 = P_1^{max}$ and $V_1 = 9$.

According to the above method, we can discretize charging power for all sensor nodes when MC stops at a location. After discretization, effective charging area C_e can be divided into multiple sectors and each sector can be denoted as S_g. The sector S_g is constructed by orientation angle vectors, and we use $v_i^{S_g}$ to represent the largest vector's sequence number near S_g for node n_i. In Figure 9, we give an example for better comprehension. The sector S_g is constructed by $\vec{o_1^0}$ and $\vec{o_1^1}$ of n_1, and S_g is contained in the sector that constructed by $\vec{o_2^3}$ and $\vec{o_2^4}$ of n_2. For node n_1 and n_2, $v_1^{S_g} = 1$, $v_2^{S_g} = 4$. Besides, due to the characteristic of directional charging, n_3 will not receive notable energy when MC's orientation angles are within S_g, and thus, we set the sequence number as a negative number in this case, i.e. $v_3^{S_g} < 0$.

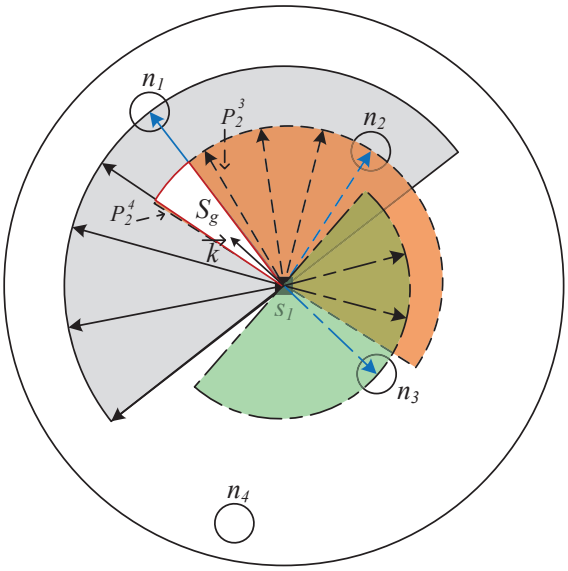

Fig. 9. An example of discretized charging orientation angles in a charging area.

For each orientation angle vector $\vec{k}$ in sector S_g, it has different charging power for node n_i. Nevertheless, the charging power under any orientation angle vector $\vec{k}$ in sector S_g satisfies:

$$P_i^{v_i^{S_g}} \le P_i^k \le P_i^{v_i^{S_g}-1} \ . \tag{17}$$

For the charging power P_i^k, it has a tight lower and upper bound since

$$\frac{P_i^{v_i^{S_g}}}{P_i^{v_i^{S_g}-1}} = \frac{1}{1+\epsilon} \ , \tag{18}$$

and we use the lower bound to represent the charging power for node n_i, i.e., $P_i^k = P_i^{v_i^{S_g}}$. When $v_i^{S_g} < 0$, which means that the received energy of n_i can be ignored, we set $P_i^k = 0$.

Currently, we can express and bound the charging powers of all nodes under any orientation angle vector within any sector

S_g as follows: $P_{S_g} = [P_1^{v_1^{S_g}}, P_2^{v_2^{S_g}}, \ldots, P_N^{v_N^{S_g}}]$. Finally, the objective problem (see (9)) can be solved by the LP solver with finite number of alternative orientation angles. The optimal charging delay obtained by LP solver after discretization has a $\frac{1}{1-\epsilon^2}$ approximation ratio to the optimal one. The detailed proof is provided below.

Approximation Ratio Proof: To prove the optimal charging delay obtained by LP solver after discretization has a $\frac{1}{1-\epsilon^2}$ approximation ratio to the optimal solution, we first propose a theorem under a scenario that MC only stops once and only chooses one orientation angle.

Theorem 1: For any orientation angle vector $\vec{k}$ within the effective directional area of nodes, its corresponding charging power vector is P_r^* and optimal minimum charging delay is T^*. S_g is the discretized sector containing $\vec{k}$ with a given threshold ϵ, $0 < \epsilon < 1$. We calculate P_{S_g} of the sector S_g and the corresponding minimum charging delay is T_g, T_g satisfies: $T_g \leq \frac{T^*}{1-\epsilon^2}$.

Proof: We first use a suboptimal charging vector P_{sub} to represent the charging power of S_g, and the corresponding minimum charging delay is T_{sub} where $T_g \leq T_{sub}$. Next, we need to prove T_{sub} satisfies $T_{sub} \leq \frac{T^*}{1-\epsilon^2}$. According to the constraints of objective (see (10)), we have:

$$P_i \cdot \frac{T^*}{1-\epsilon^2} > P_i \cdot T^* \geq \delta_i \cdot E_s \ . \tag{19}$$

Then, the minimum charging delay T_{sub} is at most $\frac{T^*}{1-\epsilon^2}$. In conclusion, we have proved that $T_g \leq \frac{T^*}{1-\epsilon^2}$. ■

Next, we denote the theoretical optimal orientation angle vector as $\vec{o_{opt}}$, and the corresponding charging delay is T_{opt}. The optimal charging vector and the corresponding charging delay obtained by charging power discretization are denoted as P_r and T, respectively. Then, we have the second theorem:

Theorem 2: The optimal charging delay T obtained by LP solver after discretization has a $\frac{1}{1-\epsilon^2}$ approximation ratio to the optimal delay T_{opt}.

Proof: Consider a special case of *Theorem 1*, i.e., $\vec{k}$ is exactly the optimal orientation angle vector $\vec{o_{opt}}$, and the corresponding charging delay is T_{opt}. Applying the similar process, we can obtain $T \leq \hat{T}_{sub}$ where $\hat{T}_{sub}$ is a suboptimal charging delay when MC charges nodes with a suboptimal charging vector. Moreover, we can have $\hat{T}_{sub} \leq \frac{T_{opt}}{1-\epsilon^2}$. Hence, we have $T \leq \frac{T_{opt}}{1-\epsilon^2}$. ■

Finally, we will verify the correctness of approximated ratio by extensive simulations in Section V for a more general case that MC stops multiple times and chooses multiple orientation angles.

B. Orientation Angle Merging

After discretization, there are still many alternative orientation angles. For some real application scenarios, MC might not rotate such many angles due to the device limitation, or users might prefer to sacrifice some performance to reduce the computational complexity. Hence, we introduce an orientation angle merging method to further reduce search space.

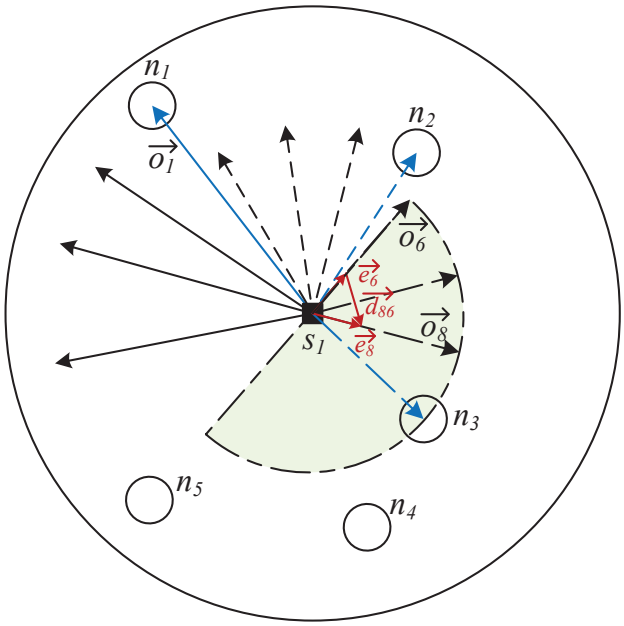

Fig. 10. Illustration for calculating d in K-means.

To merge the orientation angles, we adopt the well-known K-means clustering algorithm. The K-means algorithm first divides the input points into K initialization groups. Since nodes cannot receive power when MC rotates to the orientations outside the effective directional area, we initialize K points for every effective directional area of nodes to ensure that every node can be charged at least once. For example, n_3 cannot receive energy when MC rotates to $\vec{o_1}$ in Figure 10. Then, the algorithm divides points into the closest cluster according to the center point of each cluster. Here, we formulate distance as:

$$d = ||\vec{d_{ij}}||_2 = ||\frac{\vec{o_i}}{|\vec{o_i}|} - \frac{\vec{o_j}}{|\vec{o_j}|}||_2 \ . \tag{20}$$

As shown in Figure 10, $d = ||\frac{\vec{o_8}}{|\vec{o_8}|} - \frac{\vec{o_6}}{|\vec{o_6}|}||_2 = ||\vec{e_8} - \vec{e_6}||_2$. Next, the algorithm will recalculate the center and regroup until convergence, i.e. the center positions no longer change.

C. Computational Complexity

To solve the MAD problem, we propose discretizing and merging solution. For the discretization part, we discretize alternative orientation angles for applying LP solver to find approximated optimal orientation angles. The complexity of this part can be calculated as:

$$O(N \cdot V_i) = O(N \cdot (2\lfloor \frac{ln(\frac{1}{c}+1)}{ln(1+\epsilon)} + 1 \rfloor + 1)) = O(\frac{N}{\epsilon}) \ , \tag{21}$$

which is determined by the total sectors. For the merging part, we merge K centers in every node's effective directional area, hence, the complexity is $O(N \cdot K \cdot V_i) = O(K \cdot \frac{N}{\epsilon})$.

V. Simulations

In this section, we conduct simulations to verify the performance of our solutions.

A. Simulation Setup

Sensor nodes are randomly deployed in a $100 \times 100\ m^2$ area. The parameters of charging model in (7) are set as: $\beta = 0.1$, $\mu = 3.893$, and $c = 0.1161$, which are obtained by fitting our experiment data. Besides, we set the effective transfer distance $D = 1m$ and $\alpha \in [-\frac{\pi}{2}, \frac{\pi}{2}]$ based on our experimental results. The total energy of a sensor node is $350J$, i.e. $E_s = 350J$.

B. Baseline Setup

Since there are no approaches available to minimize charging delay for directional charging in WRSN, we introduce a baseline that adopts Set Cover concepts. In the Set Cover solution, MC always chooses the orientation angle that can maximize the number of to-be-charged sensor nodes.

In addition to the Set Cover solution, we also calculated the optimal solution for MAD with fine-grained exhaustive search via LP solver and compared the results with that of discretizing solution and merging solution.

C. Performance Comparison

In this section, we evaluate the performance of our designs by comparing it with two baselines under different charging discretization threshold ϵ, merging clusters K and the number of sensor nodes in the network N.

Impact of Charging Power Discretization Threshold ϵ: In the above sections (Section IV-C and IV-A), we have discussed that the discretization threshold ϵ will affect the computational complexity of discretizing solution and the charging delay gap between optimal solution. To analyze the performance of our solutions, we first investigate the impact of charging power discretization threshold ϵ with the network scale $N = 50$. As shown in Figure 11, we investigate the number of discretized charging orientations in one sojourn location. With the increasing of charging power discretization threshold, the number of discretized charging orientations drops very fast at first, then reveals a gradual decline trend.

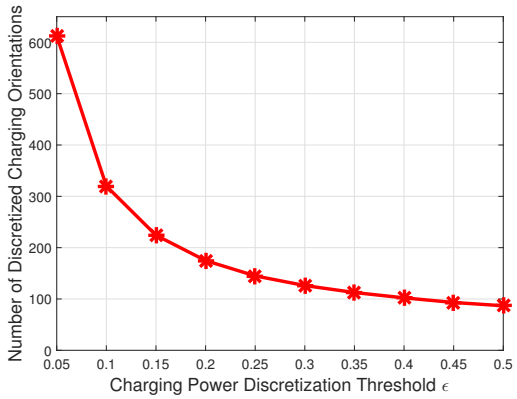

Fig. 11. Number of discretized charging orientations with varying discretization threshold ϵ.

Then, we investigate the variance of charging delay with increasing charging power discretization threshold ϵ. In Figure 12, we observe that the charging delay with optimal solution and Set Cover solution are not changed under different charging power discretization thresholds. The charging delay with discretizing solution and merging solution increase gradually with the increasing charging power discretization threshold ϵ. That is because the larger discretization threshold ϵ system sets, the looser the bounds, and accordingly, the longer the charging delay it causes.

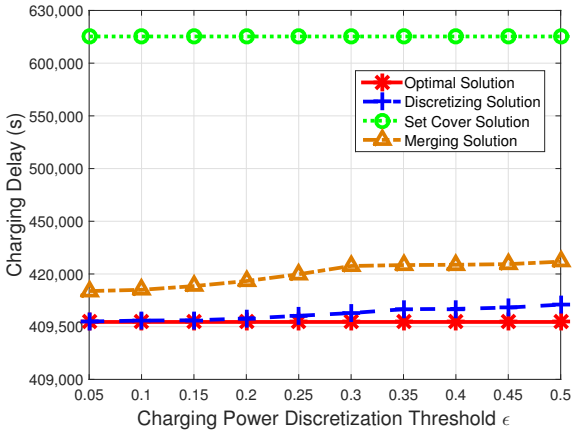

Fig. 12. Charging delay of different solutions with varying discretization threshold ϵ.

Besides, the charging delay under merging solution is longer than that under discretizing solution due to lower accuracy when depicting the charging power of sectors. Although the charging delay performs an increasing trend, it still outperforms the Set Cover baseline. The merging solution has an approximately 32% shorter charging delay.

Combining the results of two figures, we can observe that the charging delay slightly increases when the discretization threshold ϵ changes from 0.05 to 0.2. However, the number of discretized charging orientations decreases dramatically. Therefore, users can choose an appropriate discretization threshold to meet the computational overhead and charging delay requirements.

Impact of Orientation Clusters K: In this part, we investigate the impact of orientation clusters K in the merging solution. As shown in Figure 13, we can observe that the charging delay performs a decline trend. Moreover, it decreases sharply when the number of clusters K varies from 2 to approximately 30, and then gradually decreases. This is because that with the increasing of clusters, the result will be closer to that under the discretization solution.

Impact of Node Number N: In this part, we study the charging delay with different network scales under a charging power discretization threshold $\epsilon = 0.2$. Figure 14 shows the influence of node number N on the charging delay. With the increase of node number N, or so-called node density, the charging delay under all solutions increases gradually. Since multiple nodes can be charged once, which is different from the charging scheme that only one node can be charged once, the growing trend of charging delay is smoother rather than linear. Nevertheless, the charging delay under discretizing

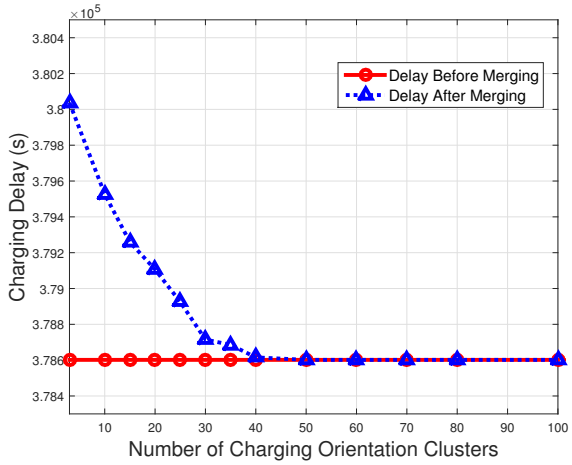

Fig. 13. Charging delay with different number of orientation clusters K.

solution and merging solution are still better than that with Set Cover solution.

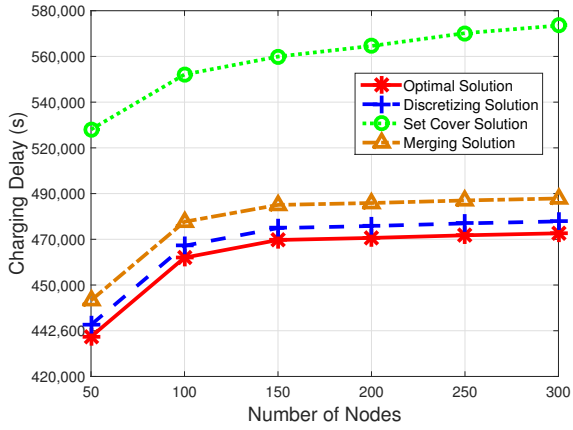

Fig. 14. Charging delay with different number of sensor nodes N.

VI. Test-bed Experiments

In this section, we conduct test-bed experiments to evaluate the performance of our design.

A. Experiment Setup

As shown in Figure 15, we use TX91501 Powercaster wireless charger and wireless rechargeable sensor nodes to conduct experiments. To make the charger move and rotate, a robot arm, implementing with a rotator, is employed as a mobile charger (see Figure 16). It is also equipped with a GPS and a camera for recording and positioning.

We conduct a test-bed experiment in the scenario that MC only needs to stop once and there are five rechargeable sensors need to be charged. The rechargeable sensors are deployed in a $100cm \times 100cm$ area and their coordinates are $(65, 56)$, $(-34, 43)$, $(40, 84)$, $(37, 62)$ and $(70, 23)$, respectively. For each sensor node, the energy threshold to work normally is $2J$. Besides, the charging power discretization threshold varies from $\epsilon = 0.1$ to $\epsilon = 0.5$ and the value of the merging clusters is $K = 5$.

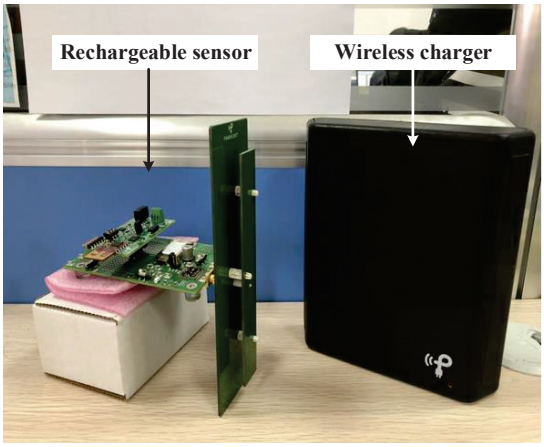

Fig. 15. TX91501 Powercaster wireless charger and wireless rechargeable sensor node.

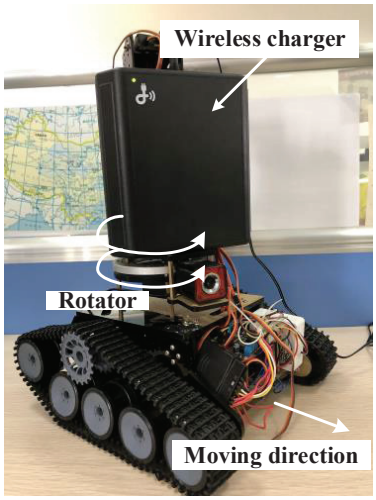

Fig. 16. A rotatable mobile robot arm.

B. Experiment Results

As shown in Figure 17, we test the charging delay under four solutions. The results coincide with the simulation results. The charging delay with discretizing solution and merging solution are at least 49% shorter than that with Set Cover solution. Besides, when $\epsilon = 0.1$, the optimal charging delay is $314.14s$ and the upper bound value of charging delay is $\frac{1}{1-0.1^2} = 317.31s$. At the same threshold value, the charging delay with discretizing solution is $314.25s$ which satisfies the bound.

VII. Conclusions

In this paper, we focus on the charging delay optimization problem for directional charging in wireless rechargeable

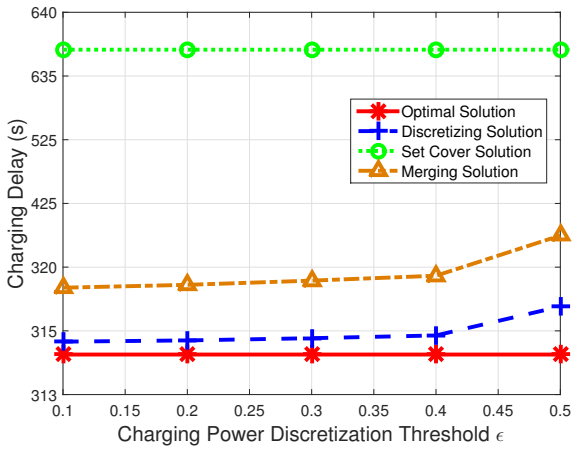

Fig. 17. Charging delay with different discretization threshold ϵ.

sensor networks. Our main contribution of this paper is on considering anisotropic energy receiving property of rechargeable sensors in directional charging. Moreover, we derive the pragmatical energy transfer model and verify the model by conducting experiments. Based on our energy transfer model, we concentrate on solving the Minimal chArging Delay (MAD) problem and formulating MAD problem as a linear programming problem. To reduce the computational complexity, we introduce the charging power discretization, which can significantly reduce the search space and bound the performance gap to the optimal one with a $\frac{1}{1-\epsilon^2}$ approximation ratio. Furthermore, we propose the merging solution to further reduce the search space. Finally, our simulation and experimental results show that our proposed schemes achieve promising performance and satisfy the approximation ratio.

Acknowledgment

This research is sponsored in part by the National Natural Science Foundation of China (61872052, 61602080, 61772113, 61733002, 61842601), National Key Research and Development Program (2017YFC0821003-2), and the "Xinghai Scholar" Program in Dalian University of Technology.

References

[1] A. Kurs, A. Karalis, R. Moffatt, J. D. Joannopoulos, P. Fisher, and M. Soljačić, "Wireless power transfer via strongly coupled magnetic resonances," *science*, vol. 317, no. 5834, pp. 83–86, 2007.

[2] H. Liu, "Maximizing efficiency of wireless power transfer with resonant inductive coupling," pp. 1–22, 2011, [Online]; Available: http://hxhl95.github.io/media/ib_ee.pdf.

[3] C. Mikeka and H. Arai, "Design issues in radio frequency energy harvesting system," in *Sustainable Energy Harvesting Technologies-Past, Present and Future*. InTech, 2011, pp. 235–257.

[4] J. R. Smith, K. P. Fishkin, B. Jiang, A. Mamishev, M. Philipose, A. D. Rea, S. Roy, and K. Sundara-Rajan, "RFID-based techniques for human-activity detection," *Communications of the ACM*, vol. 48, no. 9, pp. 39–44, 2005.

[5] Y. Shu, Y. J. Gu, and J. Chen, "Dynamic authentication with sensory information for the access control systems," *IEEE Transactions on Parallel and Distributed Systems*, vol. 25, no. 2, pp. 427–436, 2014.

[6] M. Buettner, R. Prasad, M. Philipose, and D. Wetherall, "Recognizing daily activities with rfid-based sensors," in *ACM UbiComp*, 2009, pp. 51–60.

[7] W. Du, Z. Xing, M. Li, B. He, L. H. C. Chua, and H. Miao, "Sensor placement and measurement of wind for water quality studies in urban reservoirs," *ACM Transactions on Sensor Networks*, vol. 11, no. 3, pp. 41:1–41:27, 2015.

[8] W. Du, J. C. Liando, H. Zhang, and M. Li, "When pipelines meet fountain: Fast data dissemination in wireless sensor networks," in *ACM SenSys*, 2015, pp. 365–378.

[9] W. Du, Z. Li, J. C. Liando, and M. Li, "From rateless to distanceless: Enabling sparse sensor network deployment in large areas," in *ACM SenSys*, 2014, pp. 134–147.

[10] S. Bi, C. K. Ho, and R. Zhang, "Wireless powered communication: Opportunities and challenges," *IEEE Communications Magazine*, vol. 53, no. 4, pp. 117–125, 2015.

[11] S. He, J. Chen, F. Jiang, D. K. Yau, G. Xing, and Y. Sun, "Energy provisioning in wireless rechargeable sensor networks," *IEEE Transactions on Mobile Computing*, vol. 12, no. 10, pp. 1931–1942, 2013.

[12] Z. Wang, L. Duan, and R. Zhang, "Adaptively directional wireless power transfer for large-scale sensor networks," *IEEE Journal on Selected Areas in Communications*, vol. 34, no. 5, pp. 1785–1800, 2016.

[13] L. Fu, P. Cheng, Y. Gu, J. Chen, and T. He, "Optimal charging in wireless rechargeable sensor networks," *IEEE Transactions on Vehicular Technology*, vol. 65, no. 1, pp. 278–291, 2016.

[14] S. Zhang, Z. Qian, J. Wu, F. Kong, and S. Lu, "Optimizing itinerary selection and charging association for mobile chargers," *IEEE Transactions on Mobile Computing*, vol. 16, no. 10, pp. 2833–2846, 2017.

[15] P. Zhou, C. Wang, and Y. Yang, "Leveraging target k-coverage in wireless rechargeable sensor networks," in *IEEE ICDCS*, 2017, pp. 1291–1300.

[16] S. Silver, *Microwave antenna theory and design*. IET, 1949, no. 19.

[17] H. Dai, X. Wang, A. X. Liu, H. Ma, and G. Chen, "Optimizing wireless charger placement for directional charging," in *IEEE INFOCOM*, 2017, pp. 1–9.

[18] S. Zhang, Z. Qian, F. Kong, J. Wu, and S. Lu, "P3: Joint optimization of charger placement and power allocation for wireless power transfer," in *IEEE INFOCOM*, 2015, pp. 2344–2352.

[19] S. Li, L. Fu, S. He, and Y. Sun, "Near-optimal co-deployment of chargers and sink stations in rechargeable sensor networks," *ACM Transactions on Embedded Computing Systems*, vol. 17, no. 1, pp. 10:1–10:19, 2017.

[20] C. Lin, J. Zhou, C. Guo, H. Song, G. Wu, and M. S. Obaidat, "TSCA: A temporal-spatial real-time charging scheduling algorithm for on-demand architecture in wireless rechargeable sensor networks," *IEEE Transactions on Mobile Computing*, vol. 17, no. 1, pp. 211–224, 2018.

[21] Y. Shu, H. Yousefi, P. Cheng, J. Chen, Y. J. Gu, T. He, and K. G. Shin, "Near-optimal velocity control for mobile charging in wireless rechargeable sensor networks," *IEEE Transactions on Mobile Computing*, vol. 15, no. 7, pp. 1699–1713, 2016.

[22] Z. Liu, Z. Li, M. Li, W. Xing, and D. Lu, "Path reconstruction in dynamic wireless sensor networks using compressive sensing," in *ACM MobiHoc*, 2014, pp. 297–306.

[23] L. Xie, Y. Shi, Y. T. Hou, W. Lou, H. D. Sherali, and S. F. Midkiff, "Multi-node wireless energy charging in sensor networks," *IEEE/ACM Transactions on Networking*, vol. 23, no. 2, pp. 437–450, 2015.

[24] C. Lin, Z. Wang, J. Deng, L. Wang, J. Ren, and G. Wu, "mTS: Temporal-and spatial-collaborative charging for wireless rechargeable sensor networks with multiple vehicles," in *IEEE INFOCOM*, 2018, pp. 99–107.

[25] H. Dai, Y. Liu, G. Chen, X. Wu, T. He, A. X. Liu, and H. Ma, "Safe charging for wireless power transfer," *IEEE/ACM Transactions on Networking*, vol. 25, no. 6, pp. 3531–3544, 2017.

[26] G. Han, A. Qian, J. Jiang, N. Sun, and L. Liu, "A grid-based joint routing and charging algorithm for industrial wireless rechargeable sensor networks," *Computer Networks*, vol. 101, pp. 19–28, 2016.

[27] F. Sangare, Y. Xiao, D. Niyato, and Z. Han, "Mobile charging in wireless-powered sensor networks: optimal scheduling and experimental implementation," *IEEE Transactions on Vehicular Technology*, vol. 66, no. 8, pp. 7400–7410, 2017.

[28] K.-F. Ssu, C.-H. Ou, and H. C. Jiau, "Localization with mobile anchor points in wireless sensor networks," *IEEE Transactions on Vehicular Technology*, vol. 54, no. 3, pp. 1187–1197, 2005.

[29] G. Dantzig, *Linear programming and extensions*. Princeton university press, 2016.